

# Mechanisms of Self-Ordering of Quantum Nanostructures Grown on Nonplanar Surfaces

Giorgio Biasiol and Eli Kapon

Department of Physics, Swiss Federal Institute of Technology—EPFL, 1015 Lausanne, Switzerland  
(Received 1 June 1998)

We present an analytic model that explains the self-ordering of quantum nanostructures grown on nonplanar surfaces. Self-limiting growth in these structures results from the interplay among growth-rate anisotropy, curvature-induced capillarity, and, for alloys, entropy of mixing effects. Experimental results on self-limiting organometallic chemical vapor deposition on corrugated surfaces are in quantitative agreement with the model. The implications of the self-limiting growth characteristics on the self-ordering of quantum wells, wires, and dots are discussed. [S0031-9007(98)07220-2]

PACS numbers: 68.65.+g, 68.55.-a, 81.10.Bk, 82.65.Dp

Two- or three-dimensionally quantum-confined semiconductor structures have attracted much attention because of their interesting physical properties and potential device applications [1]. To overcome limitations in size and interface quality related to traditional lithography techniques, many efforts have been devoted to study their formation during the epitaxial process [2]. This can be accomplished if a suitable driving force is introduced to yield the desired lateral heterostructure patterning. A widely used approach in this direction is to exploit self-ordering processes on *planar surfaces*, as for strained-induced Stranski-Krastanow growth of quantum dots (QDs) [3,4]. Such techniques have the advantage that self-ordering is achieved without any surface patterning prior to growth; however, they suffer from a limited control on uniformity and deposition site due to the intrinsic random nature of the nucleation process.

Self-ordering of nanostructures on *nonplanar surfaces* has the potential for solving these problems, as the corrugated surface can provide a template for the nucleation sites. In fact, organometallic chemical vapor deposition (OMCVD) and molecular beam epitaxy (MBE) on substrates patterned with corrugations (see Fig. 1) [5,6] or with pyramidal patterns [7] have been successfully employed to fabricate uniform arrays of quantum wires (QWRs) and QDs. Despite the accurate structural control demonstrated with this approach, the understanding of the self-limiting growth mechanism on such corrugated surfaces has been essentially phenomenological [8]. Existing models can, in fact, predict only constant growth rates of thick layers on  $\mu\text{m}$ -sized facets, depending on their orientation and environment, as a result of gas-phase and surface diffusion [9,10]. The growth behavior of facets in the 10-nm scale, relevant to the self-ordering of quantum nanostructures, cannot be explained with such models, since facet-size dependent surface diffusion fluxes should be invoked to account for the self-limiting growth [11].

In this Letter we address the self-limiting growth of a corrugated surface, and establish a model that quantitatively describes the self-ordering of quantum wells (QWs), QWRs, and QDs on such patterned substrates.

The formation of surface patterns during growth relies on lateral gradients in the surface chemical potential  $\mu$ . Considering, for simplicity, variations in only one dimension ( $\xi$ ),  $\mu$  of the component  $i$  of an alloy at a growth temperature  $T$  is written as

$$\mu_i = \mu_0 + \Omega_0[\sigma_\tau(\xi)]^2/2E + \Omega_0[\gamma(\theta) + \gamma''(\theta)]\kappa(\xi) + k_B T \ln x_i(\xi), \quad (1)$$

where  $x_i$  is the mole fraction. In (1), the second term is related to the tangential surface stress  $\sigma_\tau$ ,  $E$  being the elastic modulus [4], the third one is due to the surface curvature  $\kappa$  and involves the (orientation-dependent) surface free energy  $\gamma(\theta)$  [12] (with  $\Omega_0$  the atomic volume), and the fourth one is a contribution due to the entropy of mixing [13]. Self-ordering driven by lateral gradients of stress has been discussed for the InAs/GaAs system [4]. In what follows, we consider self-ordering of lattice-matched, strain-free structures, and hence drop the strain-related term.

For faceted surface profiles, such as the one shown in Fig. 1, the curvature-related contribution to  $\mu$  in (1) can be expressed as [12,14]

$$\mu_{t,b} = \mu_0 \pm \gamma\Omega_0/l_{t,b}; \quad \mu_s = \mu_0, \quad (2)$$

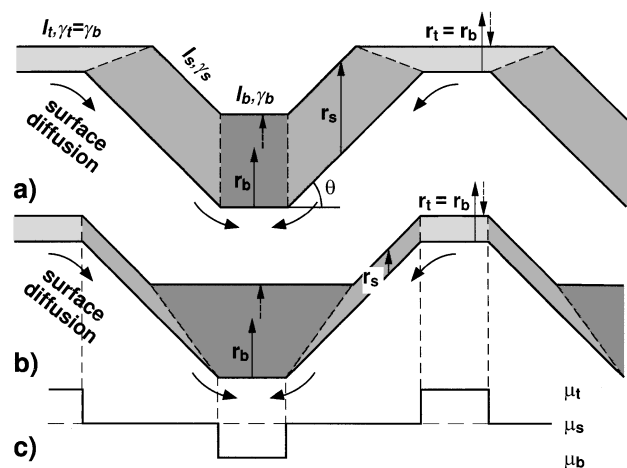


FIG. 1. Schematic groove profiles, composed of three facets (not to scale). (a) Evolution of the growth front as commonly observed in OMCVD. (b) The same for MBE. (c) Chemical potential at each facet.

where  $\theta$  is the sidewall orientation,  $\gamma = 2(\gamma_s \csc \theta - \gamma_b \cot \theta)$ ,  $+$  ( $-$ ) refers to the top (bottom) (100)-oriented facet,  $l_t$  ( $l_b$ ) is the width of the top (bottom) facet, and  $\gamma_t = \gamma_b$ . Note that  $\mu_t > \mu_0$  and  $\mu_b < \mu_0$  [see Fig. 1(c)]. This chemical potential profile determines adatom “capillarity” fluxes  $j$  towards the bottom of the groove, which increase as  $l_{t,b}$  decrease. The growth rates  $dz_i/dt$  ( $i = t, b, s$ ) at the different facets (in the growth direction) are derived from (2) using the Nernst-Einstein relation  $j_i \propto -\nabla_i \mu$  and the diffusion equation  $dz_i/dt = R_i - \Omega_0 \nabla_i j_i$ . Here the gradients  $\nabla_i$  are approximated by differences between the two boundaries of each facet [4]. Using the growth rates  $R_i = Rr_i$  on each facet in the absence of capillarity fluxes, with  $R$  being the “nominal” growth rate on a planar (100) reference sample [15], we obtain

$$\frac{dz_{t,b}}{dt} = R \left( r_b \mp r_s \frac{C}{l_{t,b}^3} \right); \quad \frac{dz_s}{dt} = Rr_s, \quad (3)$$

where  $C = 2\Omega_0 D_s \tau \gamma / k_B T$ ,  $D_s$  is the diffusion coefficient on the sidewalls,  $\tau$  is the lifetime for adatom incorporation (adatom desorption is neglected), and  $r_t = r_b$ , since these facets have the same crystallographic orientation.

Self-limiting evolution is achieved when the corners between facets propagate in the growth direction, i.e., when  $dz_t/dt = dz_s/dt$  ( $dz_b/dt = dz_s/dt$ ). This yields the self-limiting widths of the top and bottom facets  $l_{t,b}^{sl}$ ,

$$l_t^{sl} = [Cr_s/(-\Delta r)]^{1/3}; \quad l_b^{sl} = (Cr_s/\Delta r)^{1/3}, \quad (4)$$

with  $\Delta r = r_s - r_{t,b}$  representing the growth-rate anisotropy. Thus, to obtain self-limiting growth at the top (bottom) of the groove,  $\Delta r$  must be negative (positive). For  $\Delta r > 0$  the additional, capillarity-induced growth rate [dashed arrow in Fig. 1(a)] adds to the intrinsic one  $r_b$  to exactly balance  $r_s$ , since  $r_s > r_b$ . On the other hand, capillarity leads to a decrease of the top growth rate and therefore to an expansion of the top facet. The opposite behavior takes place for  $\Delta r < 0$  [see Fig. 1(b)].

Self-limiting growth at the bottom facet (with  $\Delta r > 0$ ) is obtained during GaAs/AlGaAs OMCVD on (100) substrates corrugated along the  $[01\bar{1}]$  direction [2,5]. An example is shown in Fig. 2, which displays a transmission electron microscopy (TEM) cross section of a typical cor-

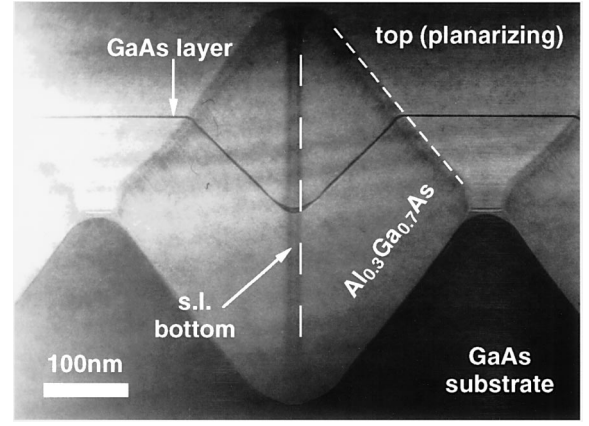


FIG. 2. TEM section of a 0.5- $\mu\text{m}$ -pitch V groove, on which a GaAs/AlGaAs heterostructure has been grown at 700 °C by low pressure OMCVD.

rugated structure (see first reference in [5] for details). The self-limiting evolution of the bottom facets is evidenced by the perpendicular propagation of the dark vertical stripe at the center of the groove (see Fig. 2), which represents Ga segregation at the nanofacets defining the bottom of the groove (so-called *vertical quantum well*, VQW) [16]. On the other hand, the boundary between the top of the mesa and the sidewalls (short-dashed line in Fig. 2) propagates towards the center of the groove, until planarization is achieved. Self-limiting growth at the top of ridges, corresponding to  $\Delta r < 0$ , has been observed in MBE growth of GaAs/AlGaAs on corrugated (100) substrates [6]. This different behavior for OMCVD and MBE, which we explain as due to the opposite sign of  $\Delta r$ , is a result of the higher dissociation rate of the precursors during OMCVD on the densely stepped groove sidewalls [10]. MBE growth, on the other hand, leads to slowly growing  $\{111\}$  A or B sidewalls [6].

We now examine the effect of the entropy of mixing term in (1) on the self-limiting profile. As a particular case, we consider the effect of the lateral variation in Al mole fraction at the  $\text{Al}_x\text{Ga}_{1-x}\text{As}$  VQW (Fig. 2). The (lower) Al mole fraction at the bottom facet can be expressed as  $x_b = x/[x(1-k) + k]$ , where  $x$  is the mole fraction at the nearby sidewalls, and  $k = 1.81 \pm 0.05$  for OMCVD growth at 700 °C [17]. Using this variation, the equations of motion for the bottom facet assume the form

$$\begin{aligned} \frac{dz_b^A}{dt} &= xR \left\{ r_b^A + \Delta r^A \left( \frac{l_b^{sl,A}}{l_b} \right)^3 + 2 \left( \frac{L_s^A}{l_b} \right)^2 \ln[x(1-k) + k] \right\}, \\ \frac{dz_b^G}{dt} &= (1-x)R \left[ r_b^G + \Delta r^G \left( \frac{l_b^{sl,G}}{l_b} \right)^3 + 2 \left( \frac{L_s^G}{l_b} \right)^2 \ln \frac{x(1-k) + k}{k} \right], \end{aligned} \quad (5)$$

with the indexes A and G referring to AlAs and GaAs growth, respectively. Equating the growth rates at the sidewalls and the bottom facet yields an equation for the self-limiting bottom facet  $l_b^{sl}$  for an alloy,

$$\frac{a}{(l_b^{sl})^3} + \frac{b}{(l_b^{sl})^2} = \Delta r(x), \quad \text{with} \quad \begin{cases} a = x\Delta r^A (l_b^{sl,A})^3 + (1-x)\Delta r^G (l_b^{sl,G})^3, \\ b = 2[x(L_s^A)^2 \ln[x(1-k) + k] + (1-x)(L_s^G)^2 \ln \frac{x(1-k) + k}{k}], \\ \Delta r(x) = x\Delta r^A + (1-x)\Delta r^G, \end{cases} \quad (6)$$

where  $l_{b,A}^{sl}$  and  $l_{b,G}^{sl}$  denote the self-limiting facet widths for the binary AlAs and GaAs composition, respectively. The self-limiting profile of an alloy is therefore determined by the interplay among the effects of capillarity ( $a$ ), entropy of mixing ( $b$ ), and growth rate anisotropy  $[\Delta r(x)]$ .

The self-limiting widths  $l_b^{sl}$  of  $\text{Al}_x\text{Ga}_{1-x}\text{As}$  as grooves grown by low pressure OMCVD were measured from TEM data for a wide range of growth parameters [18]. Figure 3(a) shows the measured self-limiting widths versus  $x$  for  $T = 700^\circ\text{C}$ . Using the measured parameters  $l_{b,G}^{sl} = 129 \pm 3$  nm,  $l_{b,A}^{sl} = 9.1 \pm 0.1$  nm, and  $\Delta r^G = 0.22 \pm 0.05$  [19], we fitted the experimental values with the solution of (6), leaving  $L_s^G$  as the only fit parameter [20], and finding  $L_s^G = 175 \pm 20$  nm. This value is lower than the one estimated on (100) surfaces [21], as expected for a densely stepped, high-index facet. To estimate the importance of the entropy effects, we also represent by the shaded area in Fig. 3(a) the best fits for  $l_b^{sl}$  neglecting the term ( $b$ ) in (6) and setting  $\Delta r^G = 0.22$ , with the boundaries corresponding to the extreme cases  $\Delta r^A = 1$  (long-dashed line) or  $\Delta r^A = 0$  (short-dashed line). The measured alloy self-limiting widths are systematically smaller than the ones predicted neglecting the entropy term.

Assuming an Arrhenius temperature dependence of  $D_s = D_0 \exp(-E_B/k_B T)$ , with  $E_B$  the diffusion

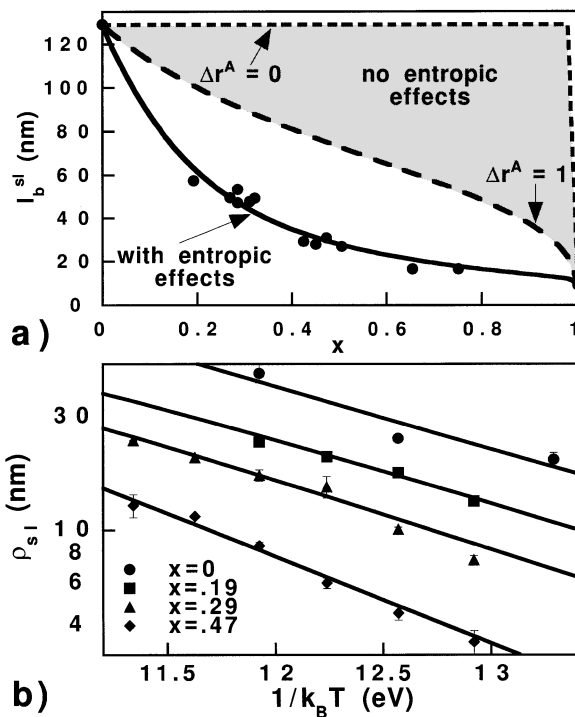


FIG. 3. (a) Measured  $l_b^{sl}$  as a function of  $x$  for  $T = 700^\circ\text{C}$ . The solid line is a fit of the measured values with the function defined in (6). The shaded region shows how the profile width would depend on  $x$  in the absence of entropy of mixing effects. (b) Arrhenius plot of  $\rho_{sl}$ , measured in  $\text{Al}_x\text{Ga}_{1-x}\text{As}$  with  $0 < x < 0.47$ .

barrier on the sidewalls perpendicular to the groove axis, (4) predicts a dependence essentially of the form  $\exp(-E_B/3k_B T)$  for  $l_b^{sl}$  in a binary. For  $\text{Al}_x\text{Ga}_{1-x}\text{As}$ , the  $T$  dependence of  $l_b^{sl}$ , given by (6), derives from the Arrhenius form of  $l_{b,A}^{sl}$ ,  $l_{b,G}^{sl}$ ,  $L_s^A$ , and  $L_s^G$ . The measured variation of  $l_b^{sl}$  with  $T$  is shown in Fig. 3(b) for  $x = 0, 0.19, 0.29$ , and  $0.47$  and for  $600 < T < 750^\circ\text{C}$ . As the bottom facets could not be readily resolved for very narrow ( $< 10$  nm) profiles, we have characterized the groove width in that case by the radius of curvature  $\rho_{sl}$  for a hyperbola tangent to the surface [8];  $\rho_{sl}$  is related to  $l_b^{sl}$  via a simple geometrical factor. The Arrhenius fit for GaAs gives  $E_B^G = 1.9 \pm 0.3$  eV. This parameter is then employed in (6) to fit the  $\text{Al}_x\text{Ga}_{1-x}\text{As}$  profiles, as a function of  $l_{b,A}^{sl}$  only. As before, we have assumed  $(L_s^G)^2 \gg (L_s^A)^2$ ,  $\Delta r^G = 0.22 \pm 0.05$  (this value does not vary significantly with  $T$ , in the range considered), and verified the insensitivity of the fit to the value of  $\Delta r^A$ . Least squares fits of the  $\text{Al}_x\text{Ga}_{1-x}\text{As}$  profiles [Fig. 3(b)] yield, consistently for the three compositions,  $E_B^A = 2.3 \pm 0.2$  eV. This difference between the GaAs and AlAs diffusion barriers is consistent with stronger Al-As bonds, as compared with Ga-As ones [22].

The evolution of the surface profile towards a self-limiting shape can be evaluated by relating the variation in the facet width to the difference in growth rates at the bottom facet and the sidewalls as  $dl_b = p(dz_b - dz_s)$  [2], where  $p$  is a factor dependent on the facet orientations ( $p = 3.75$  for our geometry). The evolution of  $l_b$  is obtained by combining (3) and (4) for a binary, or (5) and (6) for a ternary, yielding, respectively,

$$\frac{dl_b}{dz_n} = p \Delta r \left[ \left( \frac{l_b^{sl}}{l_b} \right)^3 - 1 \right], \quad (7a)$$

$$\frac{dl_b}{dz_n} = p \left\{ \Delta r(x) \left[ \left( \frac{l_b^{sl}}{l_b} \right)^3 - 1 \right] + \frac{b}{l_b^3} (l_b - l_b^{sl}) \right\}, \quad (7b)$$

where  $z_n = Rt$  is the nominal thickness. These relations show that  $l_b$  tends to expand (contract) when its size is smaller (larger) than its self-limiting one, at a rate that increases as this deviation increases [note that, since  $(L_s^G)^2 \gg (L_s^A)^2$ , the term  $b$  in Eq. (7b) is negative].

The measured evolution of  $l_b$ , starting from a self-limiting  $\text{Al}_{0.3}\text{Ga}_{0.7}\text{As}$  shape via the development of a GaAs self-limiting profile (circles) and then back to a self-limiting  $\text{Al}_{0.3}\text{Ga}_{0.7}\text{As}$  profile (squares), all taking place at  $700^\circ\text{C}$ , is displayed in Fig. 4. Both profiles evolve towards their self-limiting sizes  $l_b^{sl}$  ( $129 \pm 3$  nm for GaAs and  $31.6 \pm 1.1$  nm for  $\text{Al}_{0.3}\text{Ga}_{0.7}\text{As}$  [11]). The solid line is a numerical integration of (7a), using the experimental value  $\Delta r = 0.22$ . The evolution of the GaAs profile is well reproduced by this theoretical curve. To model the self-limiting evolution of  $\text{Al}_{0.3}\text{Ga}_{0.7}\text{As}$  (dashed line), we have used in (7b) the measured value of the growth rate anisotropy  $\Delta r(0.3) = 0.19 \pm 0.05$ , and left  $L_s^G$  as the only

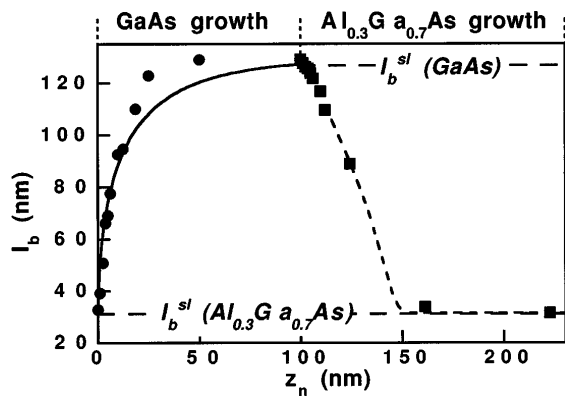


FIG. 4. Measured profile width  $l_b$  for GaAs (circles) and  $\text{Al}_{0.3}\text{Ga}_{0.7}\text{As}$  (squares) layers of increasing thickness, during evolution towards the self-limiting values  $l_b^{\text{sl}}$ . Lines are calculated curves according to Eq. (7).

fitting parameter. Least-squares fits of the experimental data then yielded  $L_s^G = 145 \pm 20$  nm, consistent with the value obtained in Fig. 3(a).

The model developed above can be employed to elucidate the self-ordering of several quantum nanostructures relying on self-limiting surface evolution. The self-limiting AlGaAs facet widths give the confinement dimension of VQW structures formed in this way on V-grooved substrates [16,17]. The fact that the self-limiting width increases with the group-III diffusion length explains directly the self-ordering of crescent-shaped QWRs grown on V-grooves [5]. Thus, growing a low band gap semiconductor layer (e.g., GaAs) characterized by a longer  $L_s$ , on a self-limiting, higher band gap surface (e.g., AlGaAs) leads to the expansion of the bottom facet and the experimentally observed formation of a QWR. The same effects also explain the self-formation of QD structures obtained by OMCVD in inverted tetrahedral pyramids [7].

In conclusion, we have shown that self-limiting epitaxial growth on nonplanar substrates results from a stable equilibrium between growth rate anisotropy on different facets composing the surface and capillarity-induced diffusion. For an alloy, the composition varies across the groove as a result of different diffusion lengths for different alloy components. Entropic effects tend, however, to counteract this nonuniform composition, thus reducing the widths of alloy self-limiting profiles. The predictions of the model quantitatively describe both the steady state and the evolution of the self-limiting surface profiles during OMCVD growth of AlGaAs on nonplanar surfaces. Strain effects could be treated in the same framework by adding the stress term in the chemical potential in (1). This model forms the basis for understanding the self-ordering of a variety of quantum nanostructures formed by growth on nonplanar substrates, including VQWs [16], crescent shaped QWRs [5], and pyramidal QDs [7].

This work was partially supported by the fonds national suisse de la recherche scientifique. We thank

A. Gustafsson and K. Leifer for the TEM data used in this work.

- [1] C. Weisbuch and B. Vinter, *Quantum Semiconductor Structures* (Academic Press, Boston, 1991).
- [2] E. Kapon, *Semicond. Semimet.* **40**, 259 (1994).
- [3] H. Drexler *et al.*, *Phys. Rev. Lett.* **73**, 2252 (1994).
- [4] Q. Xie, A. Madhukar, P. Chen, and N.P. Kobayashi, *Phys. Rev. Lett.* **75**, 2542 (1995).
- [5] A. Gustafsson, F. Reinhardt, G. Biasiol, and E. Kapon, *Appl. Phys. Lett.* **67**, 3673 (1995); X.-L. Wang, M. Ogura, and H. Matsuhata, *ibid.* **66**, 1506 (1995); G. Vermeire *et al.*, *J. Electron. Mater.* **23**, 121 (1994); A. Hartmann *et al.*, *J. Cryst. Growth* **170**, 605 (1997).
- [6] S. Koshiba *et al.*, *J. Cryst. Growth* **150**, 322 (1995).
- [7] A. Hartmann, L. Loubies, F. Reinhardt, and E. Kapon, *Appl. Phys. Lett.* **71**, 1314 (1997); S. Ishida, Y. Arakawa, and K. Wada, *ibid.* **72**, 800 (1998).
- [8] E. Kapon *et al.*, *Solid State Electron.* **40**, 1 (1996).
- [9] D. G. Coronell and K. F. Jensen, *J. Cryst. Growth* **114**, 581 (1991).
- [10] S. H. Jones and L. S. Salinas, *J. Cryst. Growth* **154**, 163 (1995).
- [11] G. Biasiol, F. Reinhardt, A. Gustafsson, and E. Kapon, *Appl. Phys. Lett.* **71**, 1831 (1997).
- [12] C. Herring, in *The Physics of Powder Metallurgy*, edited by W. E. Kingston (McGraw-Hill, New York, 1951), p. 143.
- [13] J. Y. Tsao, *Material Fundamentals of Molecular Beam Epitaxy* (Academic Press, Inc., Boston, 1993).
- [14] M. Ozdemir and A. Zangwill, *J. Vac. Sci. Technol. A* **10**, 684 (1992).
- [15] In OMCVD with TM-group-III precursors and in MBE,  $R_j$  are uniform on each facet on our length scale [2].
- [16] G. Biasiol *et al.*, *Appl. Phys. Lett.* **69**, 2710 (1996).
- [17] G. Biasiol *et al.* (to be published).
- [18] The bottom profiles, assumed here to be formed by only one facet for simplicity, are in reality composed of a (100) facet, surround by  $\{311\}$  A ones [11].
- [19] Values of  $\Delta r$  given here and later in the text were measured at the top of the mesas, for facet lengths much larger than  $l_b^{\text{sl}}$  for the given growth conditions, in order to neglect capillarity-related growth-rate variations.
- [20] Since  $(L_s^G)^2 \gg (L_s^A)^2$  [22], we have neglected in the fit the AlAs term appearing in (b) in (6), and thus any entropy-related compositional variations in the VQW are ascribed to Ga diffusion away from the bottom. No reliable estimate for  $\Delta r^A$  is available; however, the fit is very insensitive to this parameter: By changing  $\Delta r^A$  from 0 to 1, the corresponding best fit of  $L_s^G$  varied only by 7 nm, without affecting the quality of the fit. The main source of uncertainty in the fit is the error in  $\Delta r^G$ .
- [21] M. Shinohara, M. Tanimoto, H. Yokoyama, and N. Inoue, *Appl. Phys. Lett.* **65**, 1418 (1994).
- [22] A. Kley, P. Ruggerone, and M. Scheffler, *Phys. Rev. Lett.* **79**, 5278 (1997), and references therein.